Impact of Thermal Aging on the SCR Performance of Tungsten Doped CeVO4 Mixed Oxides

Sylvain Gillot, Jean-Philippe Dacquin, Christophe Dujardin, Grégory Tricot, Herve Vezin, Pascal Granger

▶ **To cite this version:**

Sylvain Gillot, Jean-Philippe Dacquin, Christophe Dujardin, Grégory Tricot, Herve Vezin, et al.. Impact of Thermal Aging on the SCR Performance of Tungsten Doped CeVO4 Mixed Oxides. Topics in Catalysis, 2018, Topics in Catalysis, 62 (1-4), pp.49-55. 10.1007/s11244-018-1082-3 . hal-03351200

HAL Id: hal-03351200
https://hal.univ-lille.fr/hal-03351200v1

Submitted on 23 Feb 2024

HAL is a multi-disciplinary open access archive for the deposit and dissemination of scientific research documents, whether they are published or not. The documents may come from teaching and research institutions in France or abroad, or from public or private research centers.

L'archive ouverte pluridisciplinaire **HAL**, est destinée au dépôt et à la diffusion de documents scientifiques de niveau recherche, publiés ou non, émanant des établissements d'enseignement et de recherche français ou étrangers, des laboratoires publics ou privés.

Submitted to the journal Topics in Catalysis in the frame of the CAPoC11

Impact of thermal aging on the SCR performance of tungsten doped $CeVO_4$ mixed oxides

S. Gillot[1], J.F. Dacquin[1], C. Dujardin[1], G. Tricot[2], H. Vezin[2], P. Granger[1]*

[1] *Univ. Lille, CNRS, Centrale Lille, ENSCL, Univ. Artois, UMR 8181 - UCCS - Unité de Catalyse et Chimie du Solide, F-59000 Lille, France*
[2] *Laboratoire de Spectrochimie Infrarouge et Raman, UMR CNRS 8516, Bâtiment C5 - UMR CNRS 8516, 59650 – Villeneuve d'Ascq, France*

* *Corresponding author :* Tel. *+33 3 20 43 49 38*
Email : pascal.granger@univ-lille.fr

Abstract

The development of more thermally stable vanadia-based SCR catalyst for combined end-of-pipe technologies, *i.e.* selective catalytic reduction catalysts wash-coated on a particulate filter, has been considered in this study. The impact of thermal aging at 850°C in wet atmosphere has been investigated on bulk W-doped $CeVO_4$ catalysts. Strong detrimental effect on the specific surface area was observed delayed by the presence of tungsten. However, they preserve a significant selective conversion depending on the surface composition with an optimal tungsten composition.

Keywords

Ammonia, $CeV_{1-x}W_xO_4$ mixed oxides, fast-SCR, Selective Catalytic Reduction, NO_x

1. Introduction

Presently, the current supported V_2O_5-WO_3/TiO_2 catalytic technology is not suited for running at high temperature especially for the development of more compact combined technologies to treat the exhaust of Diesel engines by coupling Diesel Particulate Filter (DPF) with Selective Catalytic Reduction (SCR) systems [1]. In practice, the coating of the SCR functionality on the DPF should resist to strong exotherms above 800°C during the regeneration of the DPF. In those temperature conditions, the aggregation of well-dispersed vanadate species to V_2O_5 nanoparticles would favor its sublimation at 650°C [2,3].

Up to now, promising results have been reported showing that rare earth addition to V_2O_5-WO_3/TiO_2 prevents the formation of rutile which induces a significant loss of specific surface area [4]. Iron vanadates supported on titania also led to significant enhancements of SCR performances related to an increase of defective sites and electronic disturbances between Fe^{3+} and V^{5+} [5]. As a matter of fact, surface enrichment of VO_x was often characterized and related to the gain observed in activity [5,6]. Alternative strategies were also successfully implemented through the development of vanadium free catalysts [7].

Based on those previous attempts, we found that bulk $CeVO_4$ systems [8,9] further doped with tungsten [10] exhibit interesting properties. First, vanadium is stabilized inside the zircon-type structure of $CeVO_4$ as weakly reducible V^{5+} avoiding loss of vanadium through volatilization but blocking its redox properties. They are partly restored when samples were moderately heated at 600°C. In those conditions, slight diffusion at the surface restore reducible V^{5+}/V^{4+} sites leading to unprecedented performances by comparing TOF values measured on classical supported vanadia based catalysts [8,9]. However, clustering effects might take place if the aging treatment is not properly optimised leading to the agglomeration of unselective polyvanadates. Subsequent incorporation of tungsten led to a greater stabilization of monovanadates avoiding their polymerization. The effect of tungsten has been the subject of numerous studies on supported vanadia based catalysts with sometimes controversial statements relative to the origin of its promotional effect on the catalytic properties [13]. At a first glance, tungsten strengthens the acidic properties then improving ammonia adsorption but can also alters the reducibility of VO_x species and their dispersion through dilution effect [13]. On the other hand, only few information concerns bulk catalysts. Recently we found that tungsten would preferentially play the role of stabilizer [10]. Similarly to vanadium, tungsten in the bulk structure would diffuse more readily then leading to significant surface enrichment. Accordingly, WO_x species would act as spacer preserving the dispersion of monomeric vanadate species recognized for their high selectivity. In this study we

have investigated the stability of $CeV_{1-x}W_xO_4$ aged at much higher temperatures which correspond to the conditions typically encountered during exotherms generated by the regeneration of DPF.

2. Experimental

$CeV_{1-x}W_xO_4$ samples were prepared according to a classical hydrothermal route at 180°C earlier described [9] with x varying in the range 0-0.15. The aging procedure consisted in exposing the samples at 850°C in wet atmosphere, i.e. air containing 10 vol.% H_2O. The bulk properties of the catalysts were investigated by X-Ray diffraction (XRD) by using on a Bruker AXS D8 Advance diffractometer in Bragg-Brentano geometry fitted with a LynxEye Super Speed detector. Raman spectroscopy analysis was performed on a Labram HR Jobin Yvon spectrometer. Spectra were recorded with an excitation wavelength of 532 nm. The ^{51}V magic angle spinning nuclear magnetic resonance (MAS-NMR) experiments were performed at 210.4 MHz on a 18.8 T AVANCE III Bruker NMR spectrometer with a 0.5 μs pulse length (corresponding to a $\pi/12$ flip angle), 1024-2048 transients, a recycled delay of 0.5 s and $VOCl_3$ solution as 0 ppm reference. Continuous wave electronic paramagnetic resonance (CW-EPR) experiments were measured on an X-band ELEXYS E580 Bruker spectrometer at room temperature with 256 transients, 2 mW of microwave power and 2 G of modulation amplitude. Specific surface area was measured by N_2 physisorption measurements at -196°C with a Flowsorb III device on cleaned samples after heating at 100°C under a flow of helium at ambient pressure. The surface composition was analyzed by X-ray Photoelectron Spectroscopy (XPS) analysis on an AXIS Ultra DLD Kratos spectrometer fitted with a mono-chromatized aluminium source for excitation (150 W).

Temperature-Programmed Reaction (TPR) experiments were carried out in the temperature range 120°C-550°C in a fixed bed flow reactor on 80 mg of catalyst in powder form diluted in 1 g SiC. The reaction mixture was composed of 400 ppm NH_3, 400 ppm NO_x, 8 vol.% O_2, 10 vol.% CO_2, 10% H_2O diluted in He with NO/NO_x ratio adjusted to 0.5 in fast SCR conditions. The total flow rate was fixed at 20 $L.h^{-1}$ corresponding to a space velocity of 4×10^{-3} $g.h.L^{-1}$. N_2 and N_2O concentrations were monitored by online Varian CP-4900 μGC analyses after separation of the reactants and products on two distinct columns (molecular sieve 5Å and porapak Q). NO_x ($NO+NO_2$) concentrations were measured by using a Thermo Scientific Model 42*i*-HL IR spectrometer.

3. Results and Discussion

3.1. Impact of aging on the bulk properties $CeV_{1-x}W_xO_4$

Freshly-prepared and aged samples are compared in Fig. 1A and B, respectively. As observed XRD patterns are dominated by the typical (200), (112) and (312) reflections at 2θ = 32.3 and 47.8° characteristic of the tetragonal structure of $CeVO_4$ (JCPDS PDF 12-0757). As earlier discussed [10], the shift observed on the reflections to higher 2θ values reflects the substitution of V^{5+} by W^{6+}. Additional reflections are also distinguishable ascribed to the cubic structure of CeO_2 (JCPDS PDF 34-0394). After aging, all XRD peaks become narrower reflecting a greater crystallinity. The tetragonal structure still predominates on aged samples. Interestingly, the shift previously observed has disappeared. Additional reflections also appear distinctly at 2θ = 25.5°, 26.0°, 26.6 and 48.5° on highly loaded tungsten samples ascribed to the formation of $Ce_4W_9O_{33}$ (JCPDS PDF 25-0192) [32,33]. The estimates of average crystallite size diameter by using the Scherrer equation (see Table 1) indicate a sharp increase in the crystallite size and a weak crystallite size dependency of tungsten loading.

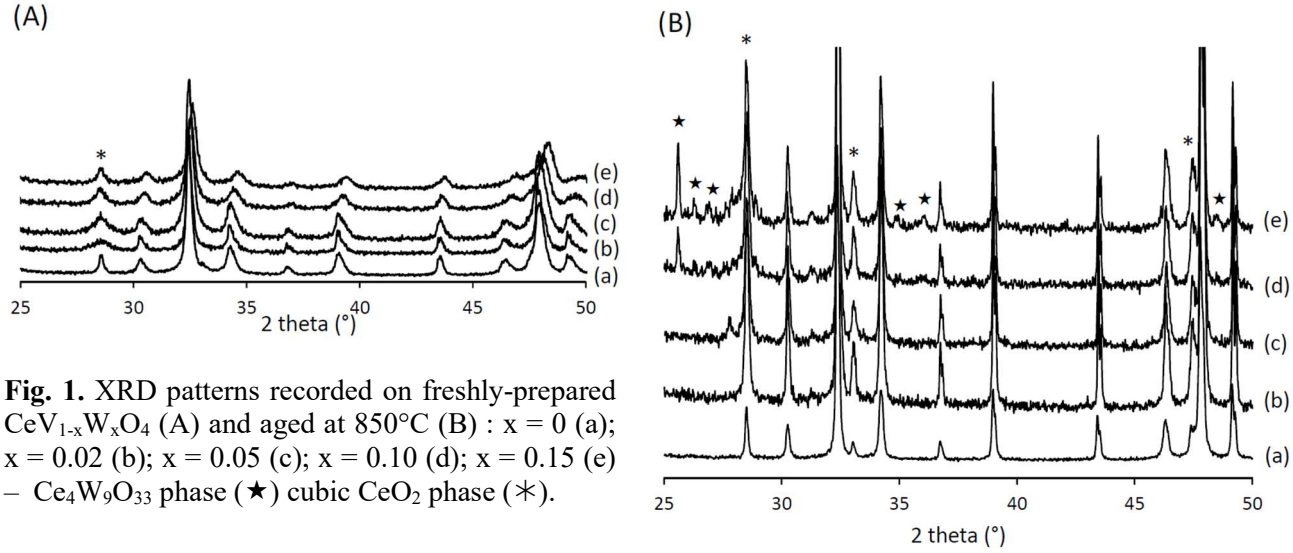

Fig. 1. XRD patterns recorded on freshly-prepared $CeV_{1-x}W_xO_4$ (A) and aged at 850°C (B) : x = 0 (a); x = 0.02 (b); x = 0.05 (c); x = 0.10 (d); x = 0.15 (e) – $Ce_4W_9O_{33}$ phase (★) cubic CeO_2 phase (∗).

Raman spectra recorded on aged $CeV_{1-x}W_xO_4$ samples are collected in Fig. 2. The characteristic Raman line of bulk V_2O_5 should appear at 994 cm^{-1} and below 800 cm^{-1} related to terminal V=O bond and V-O-V structure associated to the symmetric and antisymmetric stretching vibration modes of polyvanadate species [14,15]. As seen, they are not observed on $CeV_{1-x}W_xO_4$ suggesting the absence of bulk segregation of V_2O_5. The cubic fluorite structure CeO_2 is commonly characterized by an unique narrow band at 466 cm^{-1} assigned to F_{2g} vibration. Raman lines at 261, 383, 788, 800 and 863 cm^{-1} are characteristic of the tetragonal structure of $CeV_{1-x}W_xO_4$ [16]. The breathing mode of VO_4^{3-} with vanadium in tetrahedral coordination environment is characterized by the Raman line at 863 cm^{-1}. The Raman lines at 800 and 788 cm^{-1} correspond to the E_g and B_{2g} antisymetric stretching modes of vanadate whereas the active modes at 467 and 383 cm^{-1} can be assigned to the B_{2g} and B_{1g} deformations. As earlier found, there is no Raman line associated to WO_3 [17]. On the other hand, the weak contributions at 925 and 950 cm^{-1} for the compositions x >

0.05 can be tentatively associated to to the formation of well-crystallized $Ce_2(WO_4)_3$ [17] which seems in relative good agreement with XRD measurements detecting the presence of Ce-W mixed oxide.

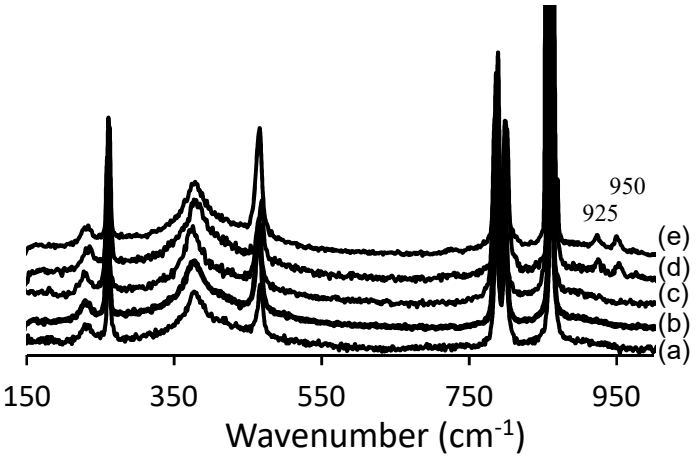

Fig. 2. Raman spectra recorded on $CeV_{1-x}W_xO_4$ aged at 850°C : x = 0 (a); x = 0.02 (b); x = 0.05 (c); x = 0.10 (d); x = 0.15 (e).

^{51}V NMR and EPR spectroscopy provide complementary information to XRD analysis and the segregation of paramagnetic V(IV) species. ^{51}V NMR spectra illustrated in Figs. 3(A) and (B) exhibit similar spectral features than those earlier discussed on samples aged at 600°C [10]. As observed on fresh samples, a shielding effect is observed for the main signal reasonably explained by the substitution of vanadium by tungsten in tetrahedral symmetry likely induced by structural distortions. On the other hand, this effect disappears with the absence of discernible shift observed on the spectra of aged samples (Fig. 3(B)) which suggests less constraint possibly related to tungsten exsolution. Let us note that this explanation matches correctly with XRD analysis. It is also noteworthy that the NMR resonances are thinner after ageing at 850°C supporting the better crystallinity of the materials. No signal characteristic of V_2O_5 is observed in the NMR analysis indicating the absence of bulk segregation of vanadium oxide. We previously shown that EPR analysis can provide complementary information emphasizing the partial transformation of weakly reducible V^{5+} stabilized in the zircon-type structure to more reducible species through the detection of paramagnetic V(IV) species which exhibit a characteristic 8 lines isotropic signals. As illustrated, in Fig. 3(D), we can observe a weak poor resolved signal (g = 1.98) arising from presence of small content of V(IV). However for the other aged catalysts such hyperfine structure does not appear indicating that there is no presence of V(IV) species but also no W(V) as its electron spin should be ½ with a d^1 configuration will give a signal below g = 2. On the other hand, a broad signal with two components is observable with an anisotropic signal g = 2.20 and g = 2.08. We believe that such g value may come from an electron trapped on oxygen atom.

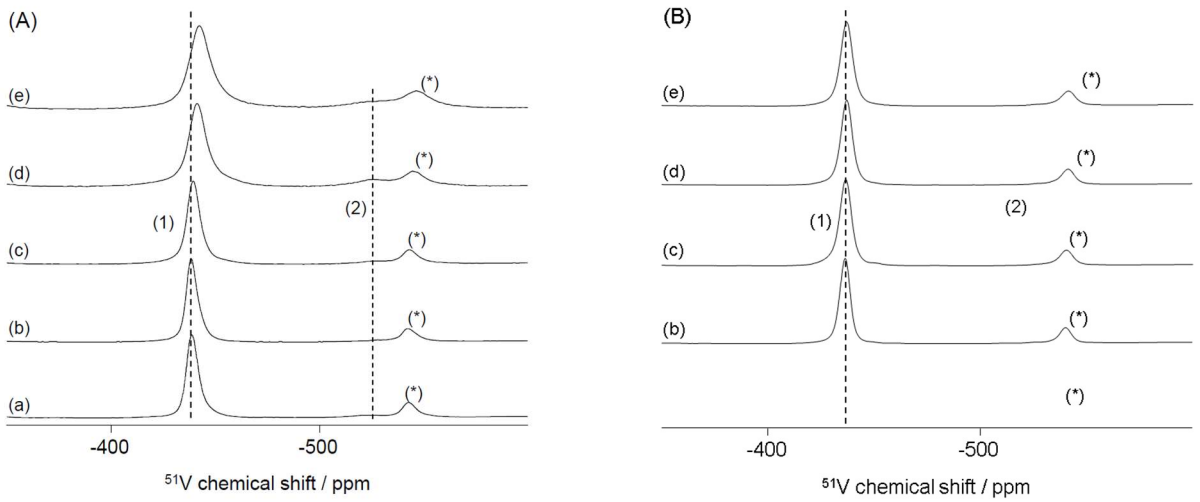

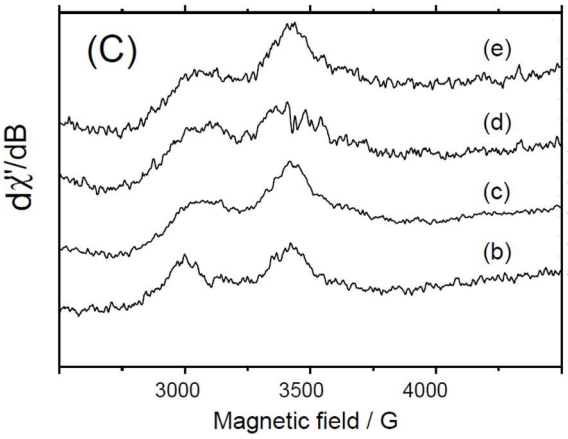

Fig. 3. ^{51}V NMR spectra recorded on fresh (A) and aged $CeV_{1-x}W_xO_4$ at 850°C (B) – x = 0 (a); x = 0.02 (b); x = 0.05 (c); x = 0.1 (d); x = 0.15 (e) – EPR spectra on aged $CeV_{1-x}W_xO_4$ (C)

Table 1
Elemental analysis, textural and structural properties of $CeV_{1-x}W_xO_4$ catalysts freshly-prepared from hydrothermal synthesis and after aging.

Catalyst		Elemental composition[a] (at.%)			Specif. Surf. Area ($m^2.g^{-1}$)	$S_{exp.}/S_{theor}$ [b]	Crystallite size d (nm)	
		Ce	V	W			$CeV_{1-x}W_xO_4$	CeO_2
$CeVO_4$	fresh	50.7	49.3	-	46.6	0.97	27	46
$CeVO_4$	aged [c]	51.6	48.4	-	< 1	0.04	96	82
$CeV_{0.98}W_{0.02}O_4$	fresh	52.9	46.0	1.1	41.0	0.82	25	n.m.
$CeV_{0.98}W_{0.02}O_4$	aged [c]	52.5	46.8	0.7	1.5	0.14	113	57
$CeV_{0.95}W_{0.05}O_4$	fresh	52.0	45.3	2.7	56.2	0.93	21	n.m.
$CeV_{0.95}W_{0.05}O_4$	aged [c]	52.3	45.7	2.0	2.1	0.78	112	40
$CeV_{0.9}W_{0.1}O_4$	fresh	51.8	42.7	5.5	57.0	0.91	20	n.m.
$CeV_{0.9}W_{0.1}O_4$	aged [c]	52.3	43.2	4.5	1.5	0.19	124	42
$CeV_{0.85}W_{0.15}O_4$	fresh	51.7	39.9	8.4	56.8	0.88	20	n.m.
$CeV_{0.85}W_{0.15}O_4$	aged [c]	51.5	41.1	7.4	1.5	0.14	122	39

[a] Energy Dispersive X-ray Spectroscopy analysis
[b] $S_{theor} = 6.10^3/(\rho.d)$
[c] After aging at 850°C in wet conditions (air + 10 vol.% H_2O)

3.2. Impact of aging on the surface properties $CeV_{1-x}W_xO_4$

Nitrogen physisorption measurements show a quasi-complete loss of the specific surface area. Probably tungsten incorporation slightly slows down this effect as exemplified on aged samples at

600°C [10]. However the severity of the thermal aging at 850°C strongly attenuates this beneficial effect with changes in the specific surface area within the margin of error. It is also obvious that this loss of surface is not strictly related to a crystal growth of $CeV_{1-x}W_xO_4$ by comparing the experimental and predicted specific surface area taking the crystallite size calculated from the Debye-Sherrer equation, i.e. the $S_{exp.}/S_{theor}$ ratio. As a matter of fact, significant segregation occurs with the detection of Ce-W mixed oxide. Pyridine adsorption led to inconclusive results because of very low density of adsorption sites for pyridine and did not allow to discuss the relative stability of Brønsted and Lewis acid sites.

XPS analysis gives some information on the surface composition and the oxidation state of Ce, V, W and O. Interestingly, the B.E. values in Table 2 remains quasi-unchanged varying within the margin of error evidencing the presence of V^{5+} and W^{6+}. As mentioned, the operating conditions led to a minor formation of CeO_2 which means that the Ce 3d spectra reflect the coexistence of Ce^{3+} and Ce^{4+}. There relative composition can be estimated through spectral decomposition leading to the calculated values of the Ce^{4+}/Ce^{3+} ratio in Table 2. As observed Ce^{3+} predominates but the aging process leads to a slight increase of Ce^{4+} species. Such changes do not seem related to the segregation of mixed Ce-W oxide but more probably to the thermal sintering of $CeV_{1-x}W_xO_4$ in greater extent than CeO_2. Such an explanation agrees with the evolution observed on the V/Ce ratio slightly decreasing. Probably the most prominent observation is given by the comparison of the surface atomic W/Ce and V/W ratio with their counterpart calculated from the elemental analysis. This comparison reflects a tremendous tungsten enrichment. As a consequence, a minimum density of VO_x is expected. Such surface tungsten enrichment was earlier observed on aged samples at 600°C but in much lower extent [10].

3.2. Catalytic performances of aged $CeV_{1-x}W_xO_4$: tentative correlations with bulk and surface structure

Fig. 4 compares the temperature-programmed NO conversion profiles vs. temperature recorded during NH_3-SCR in fast conditions on aged $CeV_{1-x}W_xO_4$ at 600°C and 850°C. As observed, a significant loss of conversion is discernible with a narrower operating window on the samples aged at the highest temperature. At a first glance, such deactivation can be reasonably explained by the sharp loss of specific surface area (around 18 $m^2.g^{-1}$ on aged sample at 600°C to 1.5 $m^2.g^{-1}$) but cannot simply explain the gain observed in conversion after tungsten incorporation. Despite, the quasi-complete loss of the specific surface area, it is remarkable that the conversion still remains significant with a maximum of 85% at 350°C on $CeV_{0.95}W_{0.05}O_4$. Typically, the volcano-type curves observed in Fig. 4(B) reflect the usual kinetic limitations. The lowest conversion at low

temperature means that the reoxidation of vanadates as active redox centers would occur slowly [18,19]. At high temperature, the competitive oxidation of ammonia to NO and N_2O becomes predominant. All those observations suggest that significant reconstructions take place at the surface modifying its composition and the nature of the active centers.

On the basis of the maximum conversions observed on the plot of the conversion curve in Fig. 4(B) the following classification can be established for the aged samples aged at 850°C $CeVO_4$ << $CeV_{0.98}W_{0.02}O_4$ ≈ $CeV_{0.85}W_{0.15}O_4$ ≈ $CeV_{0.90}W_{0.10}O_4$ << $CeV_{0.95}W_{0.05}O_4$ which differs from that reported on aged samples at 600°C with similar behavior irrespective of the tungsten composition. Hence, the superiority of $CeV_{0.95}W_{0.05}O_4$ is clearly evidenced in terms of durability and also selectivity corresponding to a broadening operating windows and a lower production of N_2O.

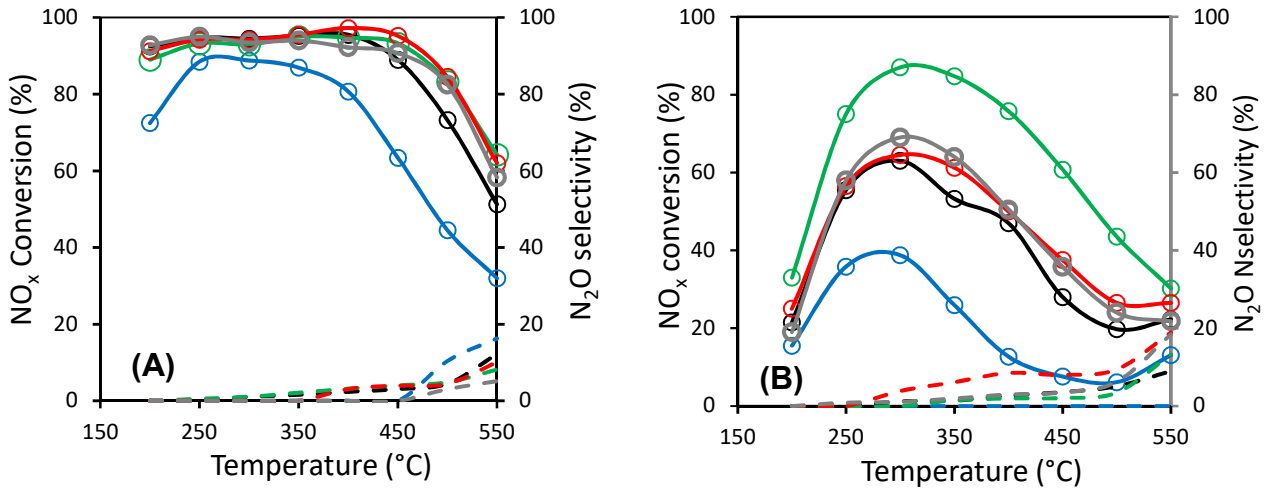

Fig. 4. Conversion (full line) and selectivity (dotted line) profiles from temperature-programmed reaction experiments in fast SCR-conditions on $CeV_{1-x}W_xO_4$ aged at 600°C **(A)** and 850°C **(B)** with : x = 0 (blue); x = 0.02 (black); x = 0.05 (green); x = 0.10 (red); x = 0.15 (grey).

Returning to the physicochemical characterization further comparisons are not trivial because the residual activity observed on aged samples depends on the combination of acidic sites to favor ammonia adsorption and redox sites to activate the SCR reaction. It was earlier demonstrated on $CeVO_4$ [8] that thermal ageing restore the redox V^{5+}/V^{4+} center, i.e monomeric and polymeric vanadates, through slight diffusion and segregation process at moderate aging temperature which led the authors to the conclusion that the reactivity of such system could be explained by the coexistence of redox V-O-V centers with weakly reducible Ce-O-V structure. Subsequent incorporation of tungsten [10] speeds up those processes but also led to more complex features because tungsten addition can modify the acidic properties through the stabilization of Brønsted acid sites or stronger Lewis acid sites as well as promotes and/or stabilizes VO_x sites. As illustrated in Figs. 1 and 2, the formation of mixed Ce-O-W structure on $CeV_{1-x}W_xO_4$ is detected for x > 0.05

which could give rise to stronger acid sites in agreement with XPS analysis showing a sharp surface tungsten enrichment. Previous investigations found that besides the acidity tungsten incorporation also improves the dispersion of Ce species and active oxygen vacancies involved in the overall catalytic process [20] which led these authors to the development of highly active vanadium free $Ce_2W_1O_x$ SCR catalysts [20] with elemental composition in agreement with XPS W/Ce ratio measured in Table 2. In our case, the identification of bulk $CeWO_x$ phase is restricted to highly loaded tungsten samples and consequently cannot explain completely the better performances obtained on $CeV_{0.95}W_{0.05}O_4$ which suggest that vanadium even at very low concentration still remains the active redox center. On the other hand, their dispersion is likely monitored by the presence of tungsten at the surface especially at high concentration. Indeed, at low tungsten concentration the tendency of VO_x to form islands could be slower whereas more intense clustering effect would prevail at higher concentration leading to more unselective catalysts especially at high temperature. In this latter case tungsten would exert compressing effect favoring the formation of vanadate aggregates which seems in the relative good agreement with the evolution of surface V/W atomic ratio.

4. Conclusions

This study deals with the impact of aging of bulk $CeV_{1-x}W_xO_4$ as potential substitute of the conventional V_2O_5-WO_3/TiO_2 technology. It was found that the stabilization of V^{5+} in tetrahedral position inside the zircon-type structure of $CeV_{1-x}W_xO_4$ preserve a loss of vanadium through volatilization. However, a drastic loss of specific surface becoming lower than 2 $m^2.g^{-1}$ was observed. Despite this detrimental effect an optimal composition $CeV_{0.95}W_{0.05}O_4$ remains still active preserving an acceptable selectivity at high temperature. As a matter of fact, the results can be explained by the contribution of tungsten inducing significant dilution effect that can slower the aggregation of isolated VO_x to unselective polymeric vanadate species at low tungsten loading whereas at high tungsten loading strong aggregation processes would occur through compressing effect.

Table 2
XPS analysis of fresh and aged $CeV_{1-x}W_xO_4$ catalysts

Catalyst	B.E. (eV) [a]			Surf. Composition [a]				
	Ce $3d_{5/2}$	V $2p_{3/2}$	W $3d_{5/2}$	V/Ce	W/Ce	V/W	Ce^{4+}/Ce^{3+}	O_α/O_β
$CeVO_4$ fresh	883.7	517.6	-	0.78 (0.97)	-	-	0.12	0.34
$CeVO_4$(850°C) [b]	883.5	517.7	-	0.82 (0.94)	-	-	0.12	0.33
$CeV_{0.98}W_{0.02}O_4$ fresh	883.4	517.7	247.9	0.96 (0.87)	0.13 (0.02)	7.4 (41.8)	0.20	0.37
$CeV_{0.98}W_{0.02}O_4$(850°C) [b]	883.3	517.7	248.0	0.78 (0.89)	0.32 (0.01)	2.5 (66.8)	0.41	0.38
$CeV_{0.95}W_{0.05}O_4$ fresh	883.4	517.6	248.0	0.89 (0.87)	0.13 (0.05)	6.8 (17.4)	0.22	0.35
$CeV_{0.95}W_{0.05}O_4$(850°C) [b]	883.4	5176	248.1	0.72 (0.87)	0.33 (0.04)	2.2 (22.9)	0.31	0.48
$CeV_{0.9}W_{0.1}O_4$ fresh	883.4	517.7	248.0	0.80 (0.82)	0.21 (0.11)	3.8 (7.5)	0.23	0.65
$CeV_{0.9}W_{0.1}O_4$(850°C) [b]	883.4	517.7	248.0	0.68 (0.83)	0.36 (0.09)	1.9 (7.5)	0.48	0.45
$CeV_{0.85}W_{0.15}O_4$ fresh	883.3	517.7	247.9	0.86 (0.77)	0.27 (0.16)	3.2 (4.8)	0.22	0.46
$CeV_{0.85}W_{0.15}O_4$(850°C) [b]	883.5	517.7	247.9	0.70 (0.80)	0.41 (0.14)	1.7 (5.6)	0.52	0.39

[a] Binding energy values and surface composition from XPS analysis

[b] After aging in wet conditions (air + 10 vol.% H_2O)

bulk compositions from elemental analysis are in brackets

Acknowledgments

This work has achieved within a research project supported by the French National Agency for Research (UreeNOx Project, Ref. ANR-11-VPTT-002). We would like to thank Laurence Burylo and Martine Trentesaux for their technical support for XRD and XPS measurements respectively.

References

[1] Granger P (2017) Catal Sci Technol 7:5195-5211.
[2] Madia G, Elsener M, Koebel M, Raimondi F, Wokaun A (2002) Appl Catal B 39:180-190.
[3] Nova I, dall'Aqua L, Lietti L, Giamello E, Forzatti P (2001) Appl Catal B 35:31-42.
[4] Larrubia Vargas MA, Casanova M, Trovarelli A, Busca G (2007) Appl Catal B 75:303-311.
[5] Liu F, He H, Lian Z, Shan W, Xie L, Asakura K, Yang W, Deng H (2013) J Catal 307:340-351.
[6] Routray K, Zhou W, Kiely CJ, Wachs IE (2011) ACS Catal 1:54-66.
[7] Li Z, Li J, Liu S, Ren X, Ma J, Su W (2015) Catal Today 258:11-16.
[8] Gillot S, Dacquin JP, Dujardin C, Tricot G, Vezin H, Granger P (2017) Appl Catal B 218:338-348.
[9] Gillot S, Dacquin JP, Dujardin C, Granger P (2016) Top Catal 59:987-995.
[10] Gillot S, Tricot G, Vezin H, Dacquin JP, Dujardin C, Granger P (2018) Appl Catal B 234:318-328.
[11] Alemany LJ, Lietti L, Ferlazzo N, Forzatti P, Busca G, Giamello E, Bregani F (1995) J Catal 155:117-130.
[12] Kompio PGWA, Brückner A, Hipler F, Manoylova O, Auer G, Mestl G, Grünert G (2017) Appl Catal B 217-365-367.
[13] Oliveri G, Ramis G, Busca G, Escribano VS (1993) J Mat Chem 3:1239-1249.
[14] Banares MA, Wachs IE (2002) J Raman Spectrosc 33:359-380.
[15] Xie S, Iglesia E, Bell AT J Phys Chem B 105 (2001) 5144-5152.
[16] Reddy BM, Khan A (2003) Langmuir 19:3025-3030.
[17] Mamede AS, Payen E, Grange P, Poncelet G, Ion A, Alifanti M, Parvulescu VI (2004) J Catal 223 :1-12.
[18] Lu X, Song C, Jia S, Tong Z, Tang X, Teng Y (2015) Chem Eng J 260:776-784.
[19] Nova I, Ciardelli C, Tronconi E, Chatterjee D, Bandl-Konrad B (2006) Catal Today 114:3-12.
[20] Shan W, Liu F, He H, Shi X, Zhang C (2012) Appl Catal B 115-116:100-106.
[21] Shan W, Liu F, He H, Shi X, Zhang C (2011) Chem. Commun. 47:8046-8048.